Acta Materialia 234 (2022) 118009

Contents lists available at ScienceDirect

Acta Materialia

journal homepage: www.elsevier.com/locate/actamat

Atomic-scale understanding of the structural evolution in TiN/AlN superlattice during nanoindentation—Part 2: Strengthening

Zhuo Chen[a], Yonghui Zheng[a,b], Yong Huang[a], Zecui Gao[c], Huaping Sheng[a], Matthias Bartosik[c,d], Paul H. Mayrhofer[c], Zaoli Zhang[a,*]

[a] Austrian Academy of Sciences, Erich Schmid Institute of Materials Science, Leoben A-8700, Austria
[b] Key Laboratory of Polar Materials and Devices (MOE), Department of Electronics, East China Normal University, Shanghai 200241, China
[c] Institute of Materials Science and Technology, TU Wien, Vienna A-1060, Austria
[d] Department of Materials Science, Montanuniversität Leoben, Leoben A-8700, Austria

ARTICLE INFO

Article history:
Received 2 March 2022
Revised 29 April 2022
Accepted 4 May 2022
Available online 5 May 2022

Keywords:
Transition metal nitride coating
Superlattice
HRTEM
Nanoindentation
Deformation
Strengthening

ABSTRACT

The mechanical properties of superlattice (SL) TMN (transition-metal nitrides) coatings with different as-deposited structures are often quite different. These differences in mechanical properties can be attributed to distinct deformation and strengthening mechanisms. Here, we discuss the strengthening mechanisms of single- and poly-crystalline SLs under nanoindentation loads. We observe that the dislocation behaviors during nanoindentation, such as dislocation accumulation and crossing interfaces, are responsible for the strengthening of single-crystalline SL coating, whereas no such pronounced strengthening is observed in the polycrystalline SL. We further reveal the monoclinic phase transformation occurring at the SL, solid solution zone, and crack tip region in the single-crystalline coating. Phase transformation alters the SL interface's structure, facilitating dislocation accumulation. Consequently, it raises the theoretical yield stress of single-crystalline coating. For polycrystalline coating, we observed a localized monoclinic phase present only near the crack tip. The current research unravels TMN SL strengthening mechanism at the atomic scale.

1. Introduction

Since the mid-1980s, the deposition method and the growth mechanism of super-hard TMN (transition-metal nitride) multilayer coatings have been reported [1–6]. For the early coatings, it was just a simple arrangement of two TMNs with different compositions alternately with the thickness of hundreds of nanometers. However, further studies show that a significant reduction of the thickness of the TMN layers (reduce to a several nanometers) and applied rock-salt/rock-salt superlattice structure could greatly enhance thin film hardness and toughness [2,3,6–11].

Previous experimental results show that multilayer coatings of various scales have significant hardness values [8,12]. This has been ascribed to different dislocation mechanisms at different scales. For the bilayer thickness with sub-micro to micro-meters, dislocations will pile up at the interface [13,14]. For the thinner period thickness, the slip of a single dislocation loop is restricted in the isolation layer, i.e., the confined layer slip (CLS) mechanism [15–17]. For the period thickness with a few nanometers, a single dislocation can cut across the interface, i.e., Koehler strengthening [18–20]. At present, among these strengthening mechanisms, the difference in shear modulus-related Koehler strengthening mechanism [18] is regarded as the main strengthening mechanism for the nanoscale periodical SL (superlattice) TMN (transition-metal nitride) coatings. However, this known strengthening mechanism is mainly affected by the intrinsic mechanical properties (i.e., shear modulus difference) of the as-deposited states and hardly involves the specific microstructure evolution during the deformation process. Therefore, to understand the underlying strengthening or softening mechanisms at deformation process, micro-scale, nanoscale and atomic-scale observations are required and essential.

By coupling FIB (focused ion beam) sectioning with C_S-corrected HRTEM (high-resolution TEM) observations, we found that nanoindentation induced single-crystalline SL large-scale interfacial mixing, dislocation accumulation, grain rotation, SL <110> slip, and poly-crystalline columnar grain boundary sliding (Part

* Corresponding author.
E-mail address: zaoli.zhang@oeaw.ac.at (Z. Zhang).

https://doi.org/10.1016/j.actamat.2022.118009

1, [21]). These deformation behaviors will essentially affect the strengthening of SLs. Moreover, detailed TEM characterization also confirmed the local phase transition behavior occurred, as predicted by theoretical simulations [22–27], which could also influence the strengthening of SL coatings. The phase transition triggers the accumulation of dislocations at the interfaces, which leads to higher theoretical yield stress than would be expected from traditional Koehler strengthening in the single-crystalline SL. In addition to the increase in hardness, based on the previous AIMD (ab initio molecular dynamics) calculations [26] and our experimental observations, the phase transition process that occurred can theoretically lead to a higher toughness, which could be a new toughening mechanism. To the end, we endeavor to clarify the SL strengthening mechanisms at the atomic scale.

2. Methods

Details of the thin film fabrication and TEM characterization methods are described in Part 1 [21].

For the dislocation density, HRTEM recorded at 600–800 Kx was used. For detailed statistical methods, please refer to our previous work in Ref. [28]. The dislocation density was obtained according to the following formula, $\rho = N/A$, where ρ is the dislocation density, N is the number of dislocations, A is the area. The strain field was calculated on the C_S-corrected HRTEM images by the geometric phase analysis (GPA) method. According to the GPA algorithm, the displacement field can be obtained by selecting two non-collinear Bragg vectors in the power spectrum generated from a HRTEM image. Shear strain map (ε_{xy}) was calculated with respect to this reference lattice defined by $\vec{g}_1 = [100]$ and $\vec{g}_2 = [010]$.

3. Results

3.1. Comparison of experimentally observed deformation

Detailed atomic-resolution studies of the deformation in SLs were shown in Part 1 [21]. To show the correlation of deformation and strengthening of SLs, here, several key points about deformation are highlighted. For the single-crystalline SL, after nanoindentation, HRTEM image exhibits the GB (grain boundary) feature in the solid solution region (as seen in Fig.1a), where the angle between two {100} planes is about 17°. This indicates that grain rotational deformation has occurred here. And, at the SL region (or undistorted region) away from the impression surface and gradually approaching the MgO substrate, the large-scale SL [110]-slip deformation occurs. The HRTEM observation (Fig. 1b) clearly demonstrates the interface structure near the slip deformation region, showing the interface is perfect and coherent. The slip deformation here is mainly formed by 1/2 a <110> full dislocation slip and crossing the SL coherent interface, and accompanied by step formation at the interface. At the edge area of the impression, we also observed a special superlattice zone with severe distorted (Fig. 1c). Therefore, there are multiple deformation mechanisms in the single-crystalline SL, as schematically shown in Fig. 1d.

In contrast, for polycrystalline SL, SAED result (selected-area electron diffraction pattern, Supplementary Fig. S1) shows there is a slight grain rotation at the indenter tip. This means, the grain rotation in polycrystalline SL is not as pronounced as in single-crystalline SL. Furthermore, the intragranular <110> slip deformation is also not the dominant deformation mechanism in polycrystalline SL (as seen in Supplementary Fig. S2). Due to the large crystallographic orientation difference in out-of-plane directions between columnar crystals (as seen in Supplementary Fig. S3), this makes it difficult that <110> slip deformation in columnar crystals extends into its adjacent columnar grains. The intragranular slipping will be limited by the width of columnar grains. Taken together, we believe that columnar grain GB sliding is the dominant deformation mode in the polycrystalline SL (Fig. 1e). The scale of other deformation behaviors, i.e., interface intermixing, interface distortion, grain rotation, and SL slipping, is considerably lower than that in the single-crystalline SL. Fig. 1f illustrates the distribution of the solid solution region, the SL interface distorted area, and the SL interface undistorted zone in the polycrystalline SL.

In short, three distinct zones (solid solution, SL distorted interfaces, and SL undistorted interfaces) are generally recognized after nanoindentation of SLs, which corresponds to distinct deformation behaviors, as summarized in schematic Fig. 1d,f.

3.2. Dislocation density variations

For the single-crystalline SL coating, EELS and HAADF observations (in Part 1 [21]) demonstrate that the tip region of the impression has a larger-scale solid solution distribution, but no severely deformed interfaces are observed (as shown in Fig. 1d). At the impression edge region, the SL interface has severe deformation and consists by dislocation pile-up. Therefore, understanding the dislocation distribution in these regions are necessary for the understanding of the hardening mechanism of SL coatings.

(i) Dislocation density variations at the impression edge.

Fig. 2a shows the transition region from the SL structure to the intermixed solid solution at the edge of the impression. The measured local dislocation distribution (plotted in Fig. 2b) reveals that the SL area possesses an extremely higher dislocation density as compared to the solid solution area, implying a dislocation accumulation in the SL area at the edge of the impression. The partially enlarged HRTEM images (Fig. 2b) also directly visualize the significant difference in the dislocation density.

(ii) Dislocation density variations beneath the impression tip.

At the tip region of the impression in the single-crystalline SL, comprehensive TEM observations showed no dislocation accumulation at the SL and solid solution (SS) interface. In Fig. 3a, a SL feature (with layered contrast) is shown on the left-hand side, where the dislocation density is significantly lower compared to the SL at the edge region (Fig. 2a). Moving to the middle of the image that the dislocation densities were statistically determined, a local increase of dislocation density at the transition area could be observed (as seen in Fig. 3b). When reaching the solid solution and inwards, the dislocation density drops rapidly, which approach to the similar value in the edge region (Fig. 2b).

At the tip area, we attribute the lower dislocation density in the SL to the higher local stress and more pronounced intermixing behavior. Close to the tip, the higher local stress will drive a larger-scale intermixing, transforming the SL into a solid solution, and consequently reducing the scale of the deformed interfaces with a high dislocation density. In other words, the larger driving force causes more adequate intermixing of the interfaces. Simultaneously, the presence of larger solid solution volume leads to more pronounced polycrystalline deformation behavior and a higher grain boundary density (as seen in the SAED result, Fig. 6 in Part 1 [21]). On the one hand, possessing a significantly high fraction of high-angle grain boundaries in the solid solution region can effectively absorb dislocations. On the other hand, the deformation (via GB sliding or grain rotation) of nanocrystalline solid solution greatly dissipates the external energy, thereby effectively protecting the SL (below the solid solution area) from further intermixing, deformation, and dislocation accumulation. Contrarily, when the solid solution area is smaller or lacks at the edge of the impression, the SL interfaces cannot be effectively protected. Thus, significant interface distortion and dislocation accumulation occur.

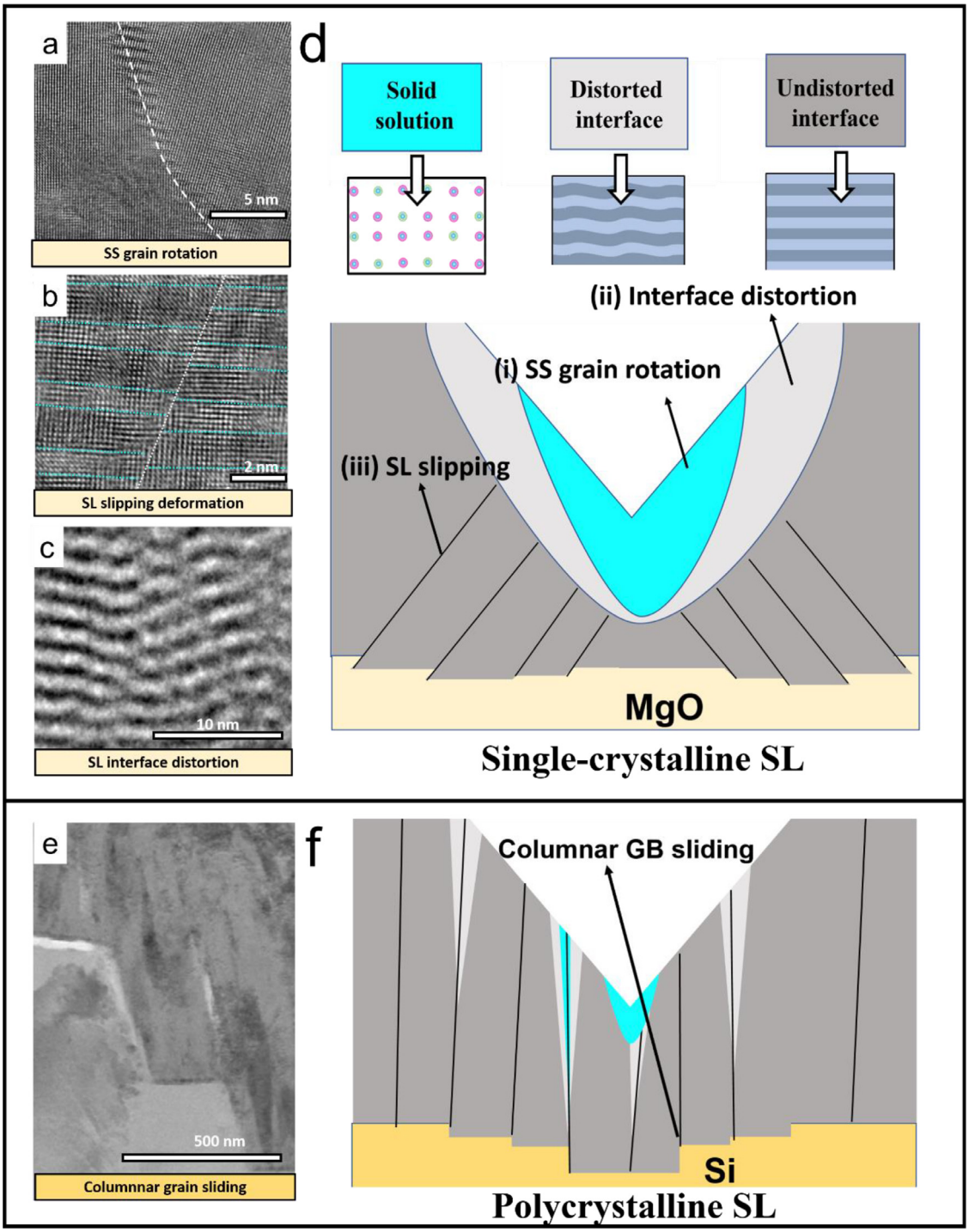

Fig. 1. a–c, HRTEM and TEM-BF images showing different deformation behaviors in an indented single-crystalline SL. **d**, A schematic distribution of three distinct zones and corresponding deformation modes in the single-crystalline SL. **e**, A STEM-BF image of the indented area clearly showing the columnar grain sliding in polycrystalline SL. **f**, A schematic distribution of three distinct zones and corresponding deformation modes in an indented polycrystalline SL. Due to the presence of native oxide, the coating is actually grown on SiO_x. Note that different color shadows designate different deformations.

For polycrystalline SL, dislocation accumulation only appears in the very vicinity of the crack or GBs, while the interior of the columnar display a lower dislocation density (shown in Part 1 [21] and Section 4.2). Thus, polycrystalline SL does not exhibit significantly larger dislocation accumulation regions than single-crystalline SL. To sum up, our results indicate that there is a competitive relationship between the different deformation mechanisms, which may affect the possible strengthening behaviors (as will be seen in the discussion).

3.3. Local phase transformation

The previous classical interface theory considers that the dislocation accumulation or dislocation pile-up in the multilayer structure generally occurs in the bilayer thickness of a few hundred nanometers [8,17,20]. For multilayer interface, when the dislocation core dimension approaches the layer thickness, the interface barrier to slip transmission decreases [12,17]. Therefore, multilayer

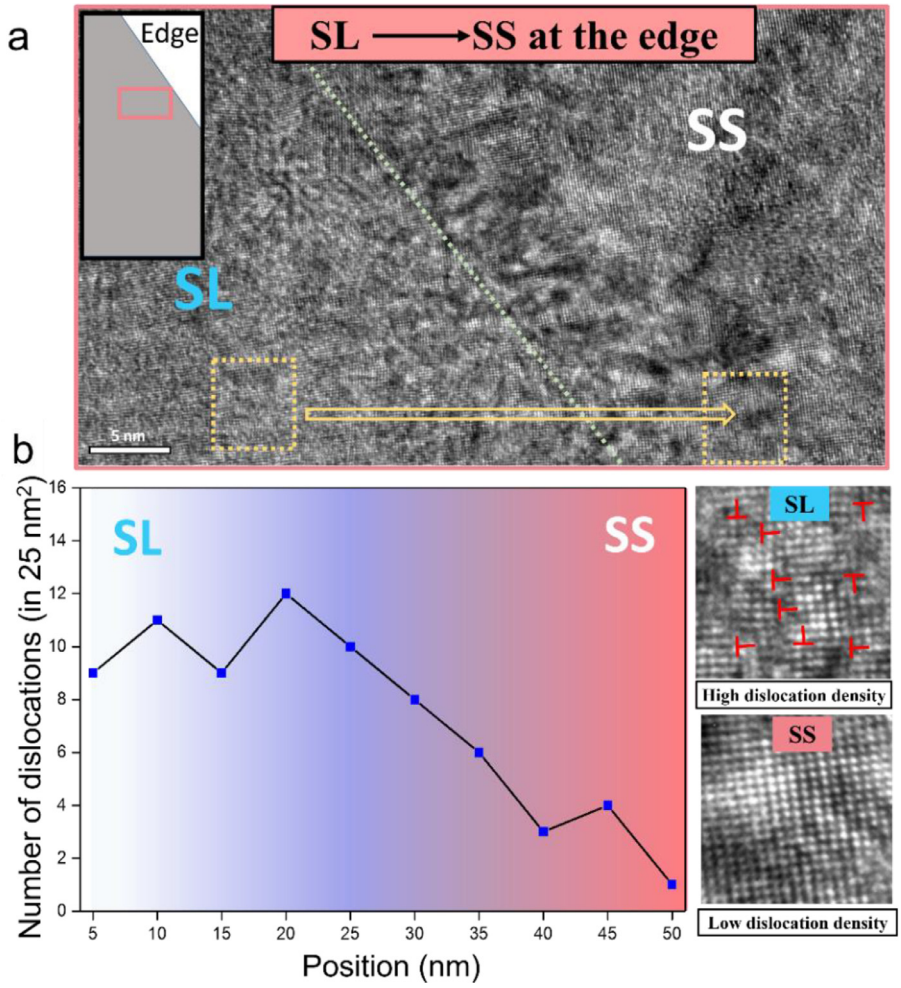

Fig. 2. a, a schematic drawing and HRTEM observation on the transition region from the solid solution to SL (separated by dotted line) at the edge of the impression of the indented single-crystalline SL. **b,** The dislocation density distribution along the indicated yellow frames in **a**, and two clippings of representative HRTEM images on the panel **b** showing the different density of dislocations. Here, only edge dislocations are counted within 5 nm × 5 nm region (yellow frames in **a**). (For interpretation of the references to colour in this figure legend, the reader is referred to the web version of this article.).

coatings with extremely small periodic thickness are not conducive to dislocation accumulation.

However, our TEM observations show results that contradict previous theories, i.e., detailed atomic-resolution observations corroborate a significant dislocation accumulation at the $\Lambda = 2.5$ nm SL coating. To explore potential explanations for the pronounced dislocation accumulation at the TiN/AlN SL interfaces, we propose that it is related to the formation of an AlN phase transition as predicted by previous simulations [23,29]. It is well known that AlN has several modifications, i.e., a stable wurtzite structure B4 with hexagonal symmetry and two metastable phases with cubic symmetry: B1 (rock-salt structure, NaCl prototype) and B3 (sphalerite structure, ZnS prototype) [30–33]. Due to the lower interfacial energy, AlN is stabilized in its metastable rocksalt structure in the as-deposited TiN/AlN SL. However, previous experiment observations (TEM results of indented TiN/AlN SL [27] and ZrN/$Zr_{0.63}Al_{0.37}N$ SL [34]), AIMD, DFT, and classical MD simulations all have shown that deformation can trigger phase transformation in AlN or Al alloyed TMN [22–27]. These phase transformations in AlN include B4–B1, B3–B1, B1–B3, and B1–B4 processes under indentation, tension, or shear deformation process. In contrast, for *rs*-TiN, DFT predicts that no phase transition occurs under deformation, and its failure mechanism is brittle cleavage [35].

(i) Phase transformation at the SL region.

As observed, the area with the severely distorted interfaces and dislocation accumulation is mostly distributed at the edge of the impression with high shear stresses. In these shear deformation regions, the monoclinic phase was exactly detected by detailed HRTEM investigations, as predicted by AlN shear deformation simulation [23]. Fig. 4a is an HRTEM image taken from the interface distortion region of the single-crystalline SL coating, where the AlN layer (with brighter contrast) exhibits obvious lattice distortions, i.e., a square lattice transforms to a quadrilateral one. The corresponding area in Fig. 4b clearly indicates that the AlN (100)/(010) lattice angle has reached 11°, corresponding to a shear strain of ~12%. In contrast, the adjacent TiN layer still maintains a square lattice and relatively lower shear strain. Using DFT simulations, Zhang and Veprek [23] demonstrated that the AlN phase transformation along the shear deformation path occurs through creating a series of monoclinic structures. Therefore, according to these simulation results, we may attribute such a high shear deformation taking place in the local AlN layer to the monoclinic phase formation (Fig. 4b, see the HRTEM image simulation results of the monoclinic phase using a space group of C2/m, monoclinic structure reference to Ref. [23], both simulated and experimental images match well).

In fact, the local phase transformation behavior that happened in the SL can reasonably explain the pronounced dislocation accumulation in the SL region. Since the crystal structure of the *rs*-TiN layer is stable during deformation, the volume expansion caused

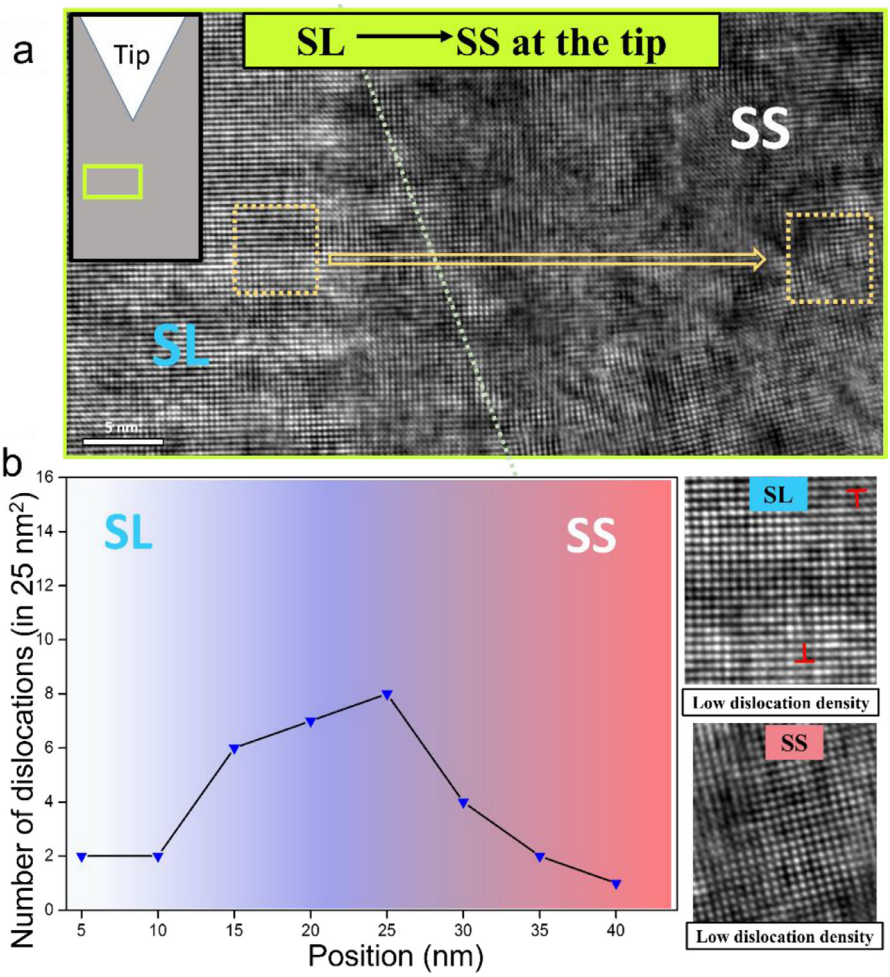

Fig. 3. **a,** a schematic drawing and HRTEM observation on the transition area from the solid solution (SS) to SL at the tip of the impression (indented single-crystalline SL). **b,** The dislocation distribution in the corresponding area (**a**, yellow frame), and two clippings of representative HRTEM images on the panel **b** showing the different density of dislocations. Here, only edge dislocations are counted within 5 nm × 5 nm region (yellow frames in **a**). Note that the difference in dislocation density beneath the tip and at the edge (referring to Fig. 2). (For interpretation of the references to colour in this figure legend, the reader is referred to the web version of this article.).

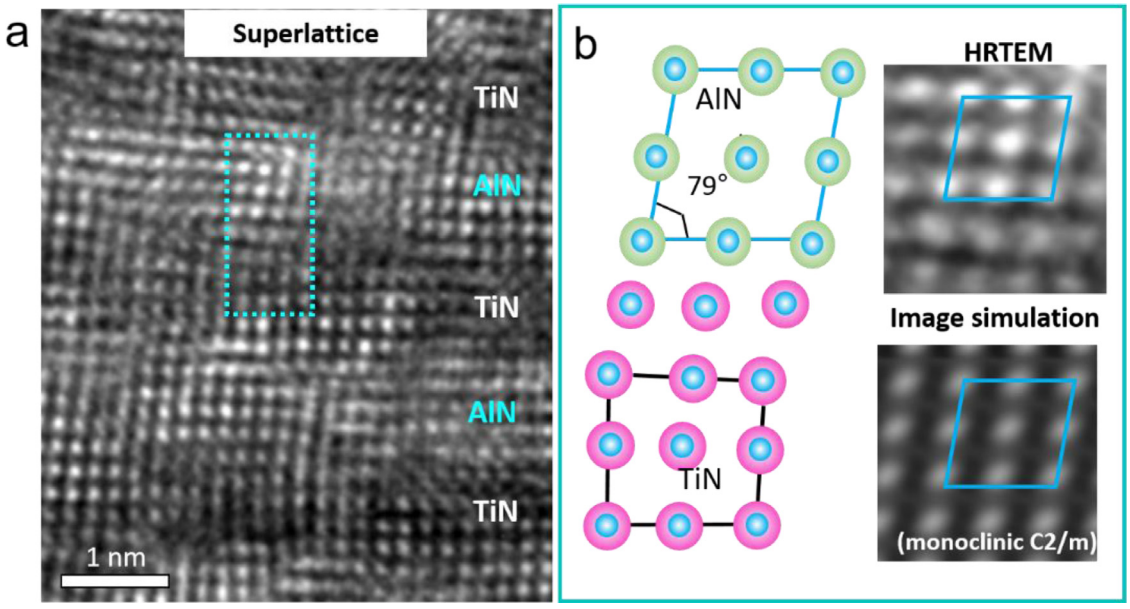

Fig. 4. **a,** A detailed HRTEM observation on a deformed interface region of indented single-crystalline SL. **b,** The monoclinic AlN and cubic TiN atomic models of the corresponding area in **a**, and a clipping of HRTEM experimental image, simulated image of the AlN layer using a monoclinic phase structure (C2/m) are shown on the panel **b**.

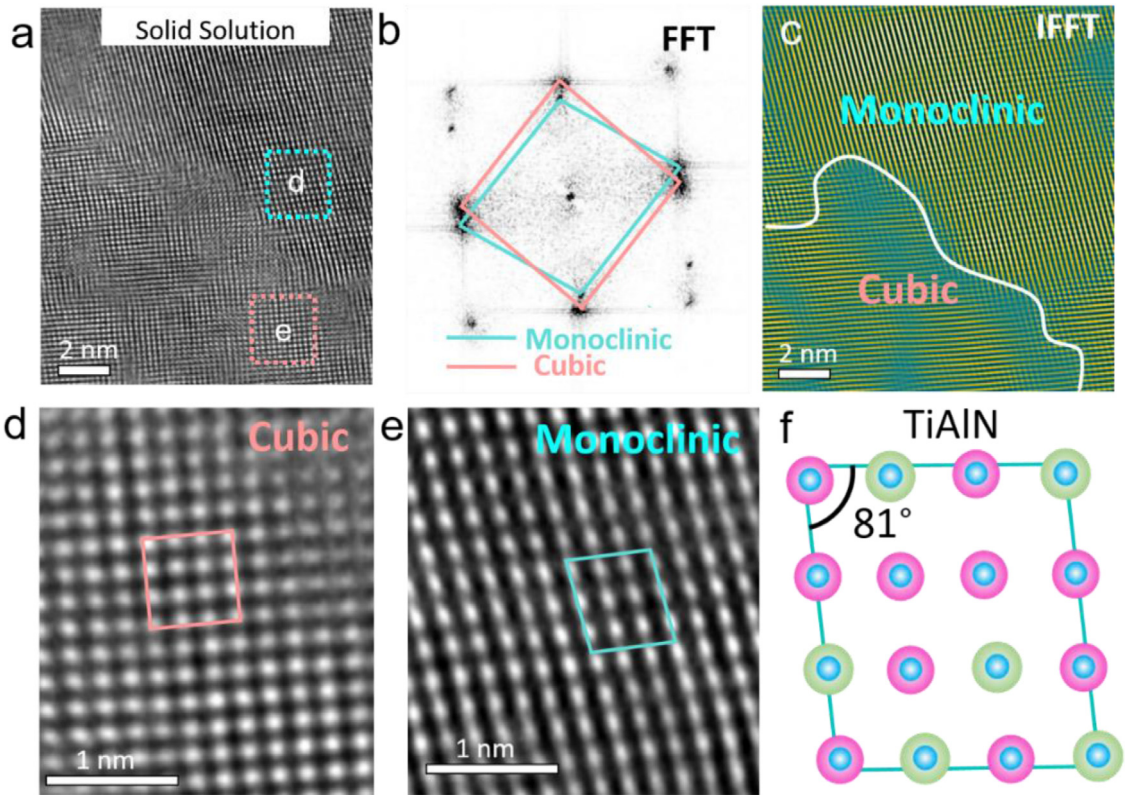

Fig. 5. **a,** Detailed HRTEM observation of the monoclinic phase in the solid solution region of the single-crystalline SL. **b,** Fast Fourier transform result of **a. c,** Inverse Fast Fourier transform of **a**, clearly showing the distribution of the cubic phase and the monoclinic phase. **d and e,** A partially enlarged image of **a f,** A model of the monoclinic solid solution is attached.

by the phase transformation in the AlN layer of the SL area will be constrained by the *rs*-TiN layer. This results in the formation of additional misfit dislocations on the interface to accommodate the lattice strain of the two layers. In addition, because the *rs*-TiN/*rs*-AlN coherent interface state is destroyed, the gliding of dislocation on the preferred slip system will be severely hindered by the rock-salt/monoclinic interface. Thus, we believe that the local phase transformation mediates the interface structure (by forming a "new" interface structure), which subsequently acts as a stronger barrier to dislocation glide, and eventually facilitates dislocations accumulation.

(ii) Phase transformation in the intermixed zone ($Ti_{1-x}Al_xN$).

Here, we also detected phase transformation in the intermixed region, i.e., $Ti_{0.67}Al_{0.33}N$ solid solution region. For $Ti_{1-x}Al_xN$, the cubic structures appeared with a critical maximum Al solubility of 0.4 to 0.9, while for the higher Al concentrations the metastable wurtzite phase could form [36–41]. Thus, the cubic structure is a stable phase for $Ti_{1-x}Al_xN$ (x = 0.33). Recent AIMD simulations by Sangiovanni et al. [26] predicted the phase transformation for $Ti_{1-x}Al_xN$ solid solution (B1-B4). In this work, although no B4 phase was observed in the solid solution region of the indented sample, HRTEM results revealed that there exists a greater extent of the monoclinic phase. Fig. 5a shows an HRTEM image of the $Ti_{0.67}Al_{0.33}N$ solid solution region, where two different crystal structures are clearly distributed. The FFT result in Fig. 5b shows the quadrilateral-shaped and cubic-shaped reflections, confirming the existence of the cubic and monoclinic structures in Fig. 5a. The result of the regional IFFT (Inverse Fast Fourier transform, Fig. 5c) shows that the upper part of the image is a monoclinic phase with a dislocation-free quadrilateral structure while the lower-left part is a cubic phase with a square lattice. The enlarged atomic resolution images (Fig. 5d,e) clearly show different lattices and angles, where the lattice angle of the monoclinic phase region is 81°. An atomic model of the monoclinic solid solution is presented in Fig. 5f accordingly. We further verify such a phase transformation by analyzing the interplanar spacing variations (Supplementary Fig. S4). The measured spacings are significantly larger in the monoclinic region than in the cubic area.

Actually, the phase transition observed in the AlN layer or solid solution region mainly exists in the single-crystal SL coating. However, it is hardly seen in the intragranular AlN layer or $Ti_{0.67}Al_{0.33}N$ solid solution region of the indented polycrystalline TiN/AlN coating. This may be relevant to the less solid solution scale and lower local stress state in polycrystalline SL, where most of the loading energy is dissipated through columnar grain boundary sliding.

(iii) Phase transformation at the crack tip.

Apart from the above observations, our HRTEM analysis revealed a monoclinic phase structure present at the crack tip (both in single-crystalline SL and poly crystalline SL). Fig. 6a is one HRTEM image taken near the edge crack (a low-mag image is inserted) in the single-crystalline SL. Two magnified atomic images (Fig. 6b,c) reveal the phase transition behavior of a cubic structure toward a monoclinic structure near the crack tip. The enlarged image (Fig. 6c) indicates that the lattice angle of the monoclinic phase region is 81°, close to the result in Fig. 5e.

Although no phase transition in the intragranular AlN layer or $Ti_{0.67}Al_{0.33}N$ solid solution region in polycrystalline SL is observed, a larger stress concentration in GBs or crack tip may trigger a localized phase transition. Fig. 6d presents the HRTEM image recorded near the crack tip in the polycrystalline SL. A cubic lattice structure retains inside the columnar crystal (Fig. 6e), whereas in the front of the crack, the monoclinic structure (with a lattice plane angle of ~82°) is also observed, as the enlarged HRTEM image (Fig. 6f) shown. In Supplementary Materials (Fig. S5), we performed fur-

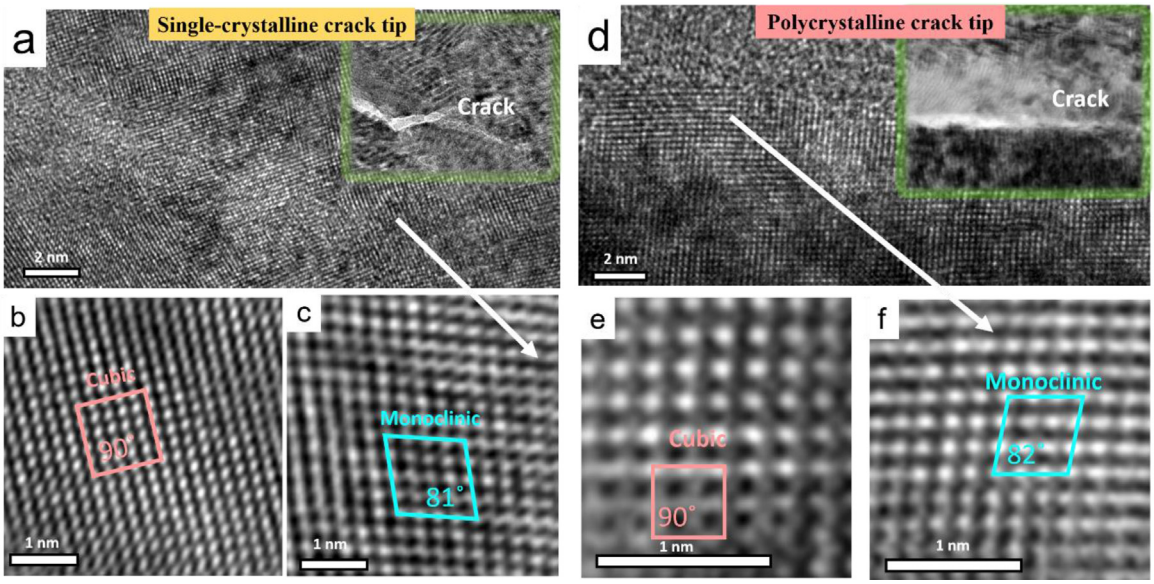

Fig. 6. a, The HRTEM observation of the crack tip in the single-crystalline SL. **b** and **c,** the phase structures at bulk and rightly in the front of the tip (labeled in **a**). **d,** The HRTEM observation of the crack tip in the polycrystalline SL. **e** and **f,** the phase structures at bulk and rightly in the front of the tip (labeled in **d**). The monoclinic phase is found near the crack (in **c, f**). Two low-magnified images (insets in **a** and **d**) indicating the crack locations.

ther HRTEM observations on monoclinic phase transition behavior near the crack in the <110> direction, and its structure and lattice-planes angle (α=γ=90°, β~81°) are consistent with those in the <100> direction (Fig. 6e).

In sum, **(1)** monoclinic phase transformation is observed in the distorted interfacial AlN layer and near-surface $Ti_{0.67}Al_{0.33}N$ solid solution region in the single-crystalline SL. **(2)** the phase transformation occurring in the distorted interfacial AlN layer facilitates dislocations accumulation. **(3)** A greater extent of phase transformation emerges in the $Ti_{0.67}Al_{0.33}N$ solid solution region of the single-crystalline SL. **(4)** the monoclinic phase structure is observed also at the crack tip region in the single-crystalline and polycrystalline SLs.

4. Discussions

4.1. On yield stress in different deformation areas

Now, it is well-established that extremely hard TMN/TMN SL coatings are obtained when grown on MgO substrates. A superhard coating with hardness values greater than 50 GPa was firstly reported in 1987 by Helmersson et al. [2] who demonstrated an enormous increase in the hardness of single-crystalline TMN SL epitaxially grown on MgO substrates by reactive magnetron sputtering. However, using different substrate materials (Si, Al_2O_3 or steel) or applying less severe deposition and growth conditions results in the growth of polycrystalline SL films. Generally, the hardness of these polycrystalline SL coatings is not as high as that of single-crystalline SL coatings [42]. Here, the 2.5 nm bilayer-period coating exhibits a higher hardness when grown on the MgO (100) substrate than on the Si (100) substrate [43]. Nevertheless, the hardness of the polycrystalline SL is obviously larger than that of the monolithic TiN (about 22 GPa) [43], implying that the polycrystalline SL still has a strengthening behavior, but is less significant than in the single-crystalline SL.

We propose that the origin of the different hardness of single-crystalline SL and polycrystalline SL is related to their different deformation behaviors. Currently, the interface hardening effect for nanoscale bilayer-thickness TMN coatings is mainly attributed to the Koehler strengthening, i.e., single dislocation crossing the interface. In this work, the presented TEM results suggest that multiple deformation mechanisms are active in the single-crystalline SL (as seen in the schematic image of Fig. 1d. These microstructures and deformation mechanisms may include SL region interface distortion, SL region slip deformation, grain rotation, and GB sliding in the solid solution region. Thus, our nanoindentation experiments confirmed that Koehler strengthening is not the sole hardening mechanism.

For the single-crystalline SL, regions with different deformation mechanisms might have completely different local stress states and dislocation behaviors, which result in different hardening or softening. Fig. 7a shows the dislocation distribution (HRTEM result) and the stress state (GPA result) of the area with interface distortion in the single-crystalline SL coatings. According to the GPA result, the local shear strain of the corresponding region may vary from -10% to +10%. We believe that the extremely high dislocation density and local stress here are mainly due to the local phase transformation in the AlN layer, which results in the interface structure evolution from the initial coherent to heterophase incoherent interface with a high misfit of lattices. On the one hand, this increases the density of misfit dislocations on the rock-salt/monoclinic interface. On the other hand, compared to a perfectly cubic/cubic coherent interface, a semi-coherent or incoherent interface with a higher stress state will make a single dislocation glide across the interface more difficult, facilitate dislocations accumulation on the 2.5 nm-bilayer-period SL interfaces (as seen in Fig. 7b).

According to the dislocation density in the deformed region, we may estimate the yield stress by Taylor's strengthening law [44], where increased yield stress (in an *rs*-TiN or AlN layer) can be expressed as:

$$\Delta\sigma = M\alpha\mu b\sqrt{\rho} \quad (1)$$

Where M is Taylor factor, α is a numerical factor (typically, in *fcc* crystal $a \approx 0.35$ [45]), μ is the shear modulus, b is the magnitude of the dislocation Burgers vector and ρ is the dislocation density. Here, the Taylor factor is 3.33 for nitrides [20], the shear modulus μ for TiN is 183 GPa [46], the Burgers vector is 0.21 nm (1/2a [100] type). Therefore, according to the dislocation density in Fig. 7a (here it is considered that the TiN layer has a similar dis-

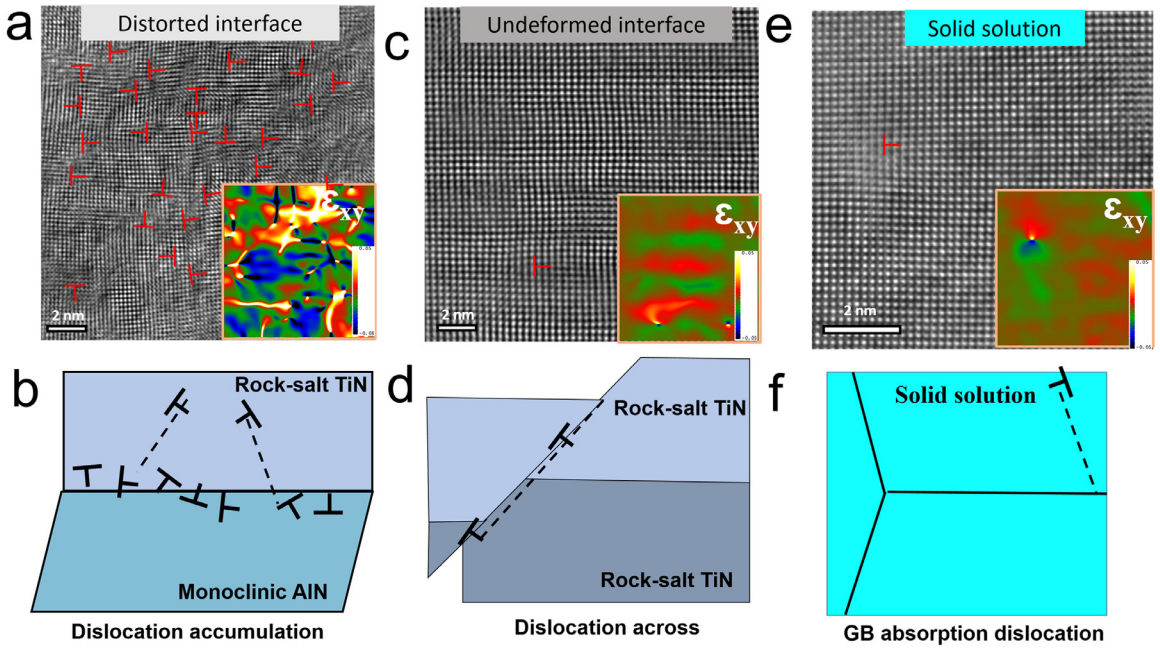

Fig. 7. **a,** A HRTEM image showing the dislocation distribution and strain field (GPA results) in the distorted interface region. **b,** a schematic diagram of dislocation behavior in the deformed interface. **c,** A HRTEM image showing the dislocation distribution and stress field (GPA results) in the un-deformed interface region. **d,** a schematic diagram of dislocation behavior in the un-deformed interface. **e**, A HRTEM image showing the dislocation distribution and stress field ε_{xy} (GPA results) in the solid solution region. **f,** a schematic diagram of the large-angle GB absorption dislocation behavior in the solid solution region.

location density to the AlN layer), the yield stress of the TiN layer will be at least increased by 16.3 GPa. For the *rs*-AlN layer (μ is 211 GPa [46]), the yield stress will further increase by 18.7 GPa.

Fig. 7c shows the dislocation distribution (HRTEM result) and the shear stress state (GPA result) for the un-deformed interface region, i.e. slip deformation region. Compared to Fig. 7a, the un-deformed interface region has a very low dislocation density (misfit dislocations of the coherent interface region) and a fully coherent stress state. Given the perfect coherent interface, a dislocation will more easily pass through the interface along the <110> direction leading to complete large-scale slip deformation (as seen in schematic image Fig. 7d and the TEM result in companion paper [21]. Therefore, the yield stress here can be described by the Koehler strengthening model. According to Koehler's theory, the maximum increased yield stress (σ) can be obtained by [18]:

$$\Delta\sigma = M\frac{\pi(\mu_1-\mu_2)}{8(\mu_1+\mu_2)}\mu\sin\theta \tag{2}$$

With consideration to the primary {110}<110> slip system, θ takes the value of 45° for the <100> SL. μ_1 *and* μ_2 are the shear modulus in different layers (in this work, μ_1 is the shear modulus of rs-AlN and μ_2 is the shear modulus of rs-TiN) Therefore, the yield stress of a single dislocation crossing the interface will increase by 12.0 GPa.

For nanoscale SLs, the influence of dislocation core should be considered. For the revised Koehler's theory, the increased yield stress can be simplified as [47]:

$$\Delta\sigma = M\frac{2\alpha(\mu_1-\mu_2)}{\pi}\sin\theta\left(\frac{b^2}{4x^2+b^2}+\frac{b}{2x}tan^{-1}\frac{2x}{b}\right) \tag{3}$$

where α is $1/4\pi$ and $(1\text{-}\nu)/4\pi$ for screw and edge dislocations ($\nu_{TiN} = 0.225; \nu_{TiN} = 0.174$ [46]), x is the distance between the interface and the dislocation. Thus, the revised yield stress of a single dislocation crossing the interface will increase by [8]:

$$M\frac{(1-\nu)(\mu_1-\mu_2)\sin\theta}{\pi^2} \le \Delta\sigma \le M\frac{(\mu_1-\mu_2)\sin\theta}{\pi^2} \tag{4}$$

Therefore, for the revised Koehler's theory, the maximum increased yield stress of a single dislocation crossing the interface will rise by ~6.4 GPa.

Based on the above analysis, in a word, dislocation accumulations lead to the increase of the yield strength in the single – crystalline SL.

4.2. On the hardness of single-crystalline and polycrystalline SL coatings

In this work, we argue that the TiN/AlN SL hardness enhancement may be also related to the interlayer phase transformation mediated Taylor's strengthening mechanism, except the other factor, i.e. Koehler strengthening. As analyzed in the previous section, in general, for the single-crystalline TiN/AlN SL, the interface distortion region with dislocation accumulation can provide a greater strengthening behavior (compared to the Koehler strengthening). This implies that the dislocation accumulations associated with the phase transformation in AlN provides a higher theoretical hardness.

In the solid solution region, due to the disappearance of the layer interfaces and the interfacial stress field (as seen in Fig. 7e and inside the GPA result), the solid solution zone will reduce the yield stress of the dislocation gliding. At the same time, since the GBs in the solid solution can effectively absorb dislocations (as seen in Fig. 7f), this causes hardly dislocation accumulation in the alloyed area (confirmed by Fig. 2). As a result, the alloying process of the interfaces thus severely suppresses Koehler's strengthening and Taylor's strengthening. And, the deformation of a larger-scale solid solution is through more grain rotations that will consume the load energy. Therefore, the intermixing of the SL interfaces is not conducive to the coating maintaining mechanical strength.

In general, the polycrystalline TiN/AlN SL's strength is not as good as the single-crystalline TiN/AlN SL coating (coatings with different bilayer periods are included) [43]. As shown in Fig. 8, the nanoindentation load/depth curves (using Berkovich and cube corner tips) indicate a higher strength for single-crystalline TiN/AlN

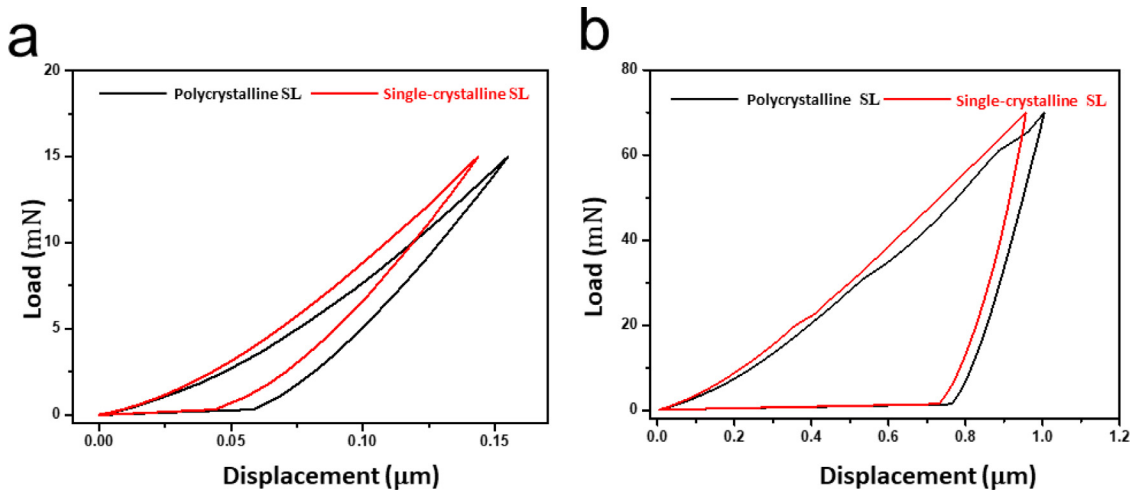

Fig. 8. a, Nanoindentation curves for the TiN/AlN films (polycrystalline and single-crystalline SL) with the Berkovich tip. **b,** Nanoindentation curves for the TiN/AlN films (polycrystalline and single-crystalline SL) with the cube corner tip.

SL, i.e., a smaller loading depth at the same loading. Furthermore, the nanoindentation load-unload curve (Fig. 8a) displays that both single-crystalline and polycrystalline SLs show the elastoplastic deformation behavior and with the similar elastic strain. The difference lies in that the single-crystalline SL has a higher elastic modulus, while the polycrystalline SL has a higher plastic strain. It could be speculated that the better plasticity in the polycrystalline SL could be attributed to its large-scale GB sliding deformation behavior.

Although polycrystalline TiN/AlN SL coating (for this work) hardness (H of 31.8 ± 0.8 GPa [43]) enhancement is lower than that of the single-crystalline TiN/AlN SL (H of 37.0 ± 0.5 GPa [43]), its hardness is still higher than that of the monolithic polycrystalline or single-crystalline coatings [2,48,49]. We consider that the deformation mechanism for the polycrystalline SL coating is dominated by columnar grain sliding along the load direction (as seen in Fig. 1f). Such a predominant sliding deformation hinders the occurrence of many other potential deformations and strengthening behavior of TiN/AlN SL, e.g., interface distortion, dislocation pile-up or dislocation crossing interfaces. Through TEM observations, we found interface distortion (Fig. 9a) and an increase in dislocation density near the GBs of the columnar grains, while the interior of the columnar grains still maintains un-deformed layered structures with a lower dislocation density (as seen in Fig. 9b,c). Due to the local increase of the dislocation density at the GBs (as seen in the schematic diagram of Fig. 9d), the coating may form immobile regions with high yield stress, thereby increasing the yield stress for GB slip. Thus, we speculate that the deformation of the interfaces near the columnar GBs can still strengthen the polycrystalline SL coating to a certain extent. However, further studies are necessary to pinpoint and quantify the relevant hardening effect in polycrystalline SL.

In a word, dislocation accumulation and crossing dominate the strengthening of single –crystalline SL while no such pronounced strengthening is observed in polycrystalline SL. Consequently, single-crystalline SL generally exhibits a higher strength.

4.3. Toughening mechanisms in TiN/AlN SLs

Previous work [43] showed that the hardness/modulus ratio in single-crystalline SL TiN/AlN SL (Λ = 2.5 nm) was ~0.093, while it was ~0.088 in polycrystalline SL. No matter single-crystalline SL and polycrystalline SL, the hardness (H)/modulus (E) ratio is generally much higher than monolithic TiN films. Empirical indicators of a high H/E value unveil that the thin film enhances toughness and wear resistance [50].

The superlattice toughening effect can be explained as the stress field at the coherent interface. The lattice parameter difference of Δa = 0.2 Å (between *rs*-TiN and *rs*-AlN, JCPDF files: 38–1420 TiN, 25–1495 *rs*-AlN) results in a coherent strain ε_c of ~5% on the *rs*-TiN/*rs*-AlN coherent interface. Therefore, the TiN layer is affected by the compressive stress, which will close the cracks and impede crack growth across the interface. For the severely distorted interface region in the single-crystalline SL, the high density of dislocations in this region leads to the stress concentration, microcrack propagation and fracture. Meanwhile, due to the destruction of the coherent interface structure (caused by local phase transformation), the lack of coherency stresses will also weaken the toughening effect of the interface. However, the volume expansion triggered by the phase transformation process may compress the surrounding area and promote the closure of other cracks, which still contributes to the toughening of the SL structure. The AIMD simulation by Koutná *et al.* showed that the local B1-B4 phase transformation of the AlN layer in the TiN/AlN SL could increase the ultimate fracture strain by about 8% under a certain bilayer thickness [27], which exemplified the phase transformation enhanced toughness in the TiN/AlN multilayer.

The formation of the solid solution zone in the single-crystalline SL is also conducive to improving the toughness. The tensile deformation simulation showed that the perfect single-crystalline $Ti_{1-x}Al_xN$ solid solution with phase transformation behavior (B1–B4) can increase its ultimate fracture strain to 50%, resulting in super toughness [26]. Although no B4 phase was observed in our indented sample, HRTEM images revealed the presence of a monoclinic $Ti_{0.67}Al_{0.33}N$ phase. The phase transformation in the solid solution can effectively relax the deformation energy, and suppress the crack initiation through effective volume expansion. Theoretically, the phase transformation from cubic to wurtzite AlN is associated with a molar volume expansion of about 20% [51]. According to our estimated results (Supplementary Fig. S6 and FFT result in Fig. 5b), the monoclinic solid solution is approximately 12–13% larger (according to two-dimensional regions) than the cubic solid solution in the projection direction. Therefore, it suggests that the formation of a monoclinic phase is still conducive to its volume expansion.

The toughening effect via the solid solution formation can be briefly summarized as follows: (i) The energy dissipation and volume expansion caused by the phase transformation of $Ti_{0.67}Al_{0.33}N$

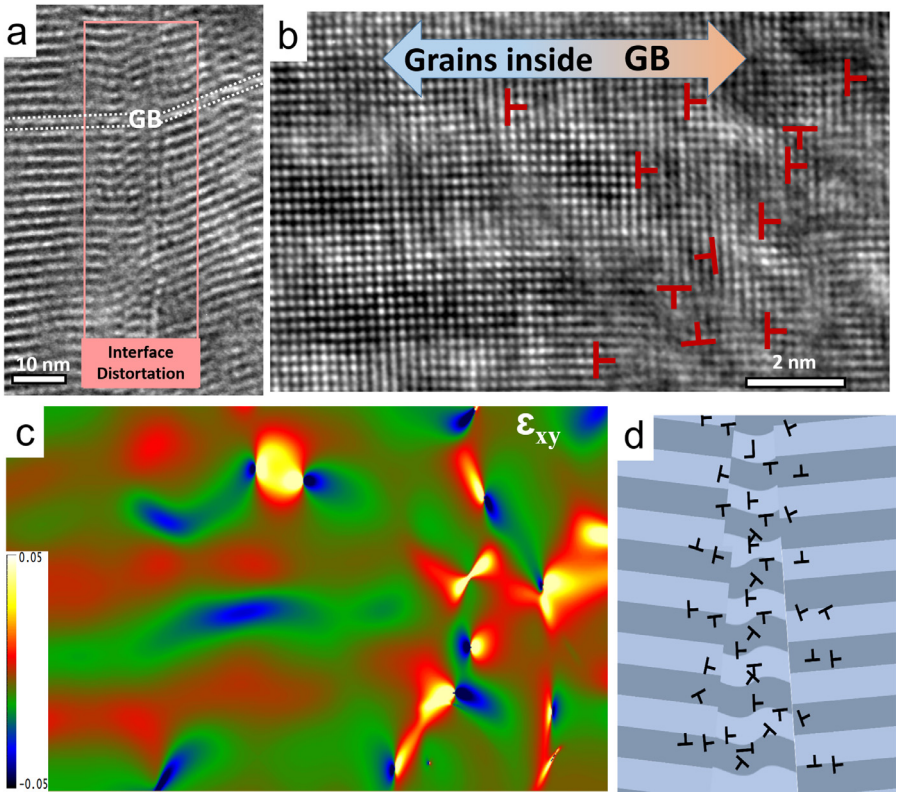

Fig. 9. a, TEM-BF image of the indented polycrystalline SL from the columnar GB region, where the labelled region shows significant interface distortions. **b,** Dislocation distribution near the GB in the indented polycrystalline SL. **c,** Strain field (GPA results of ε_{xy}) of **b.d,** An schematic drawing illustrates its deformation behavior in one columnar grain boundary.

from the cubic to the monoclinic. (ii) The formation of a ternary solid solution will also enhance the valence electron density to increase its inherent toughness [52–55]. (iii) The polycrystalline deformation behavior (Grain rotation or GB sliding) in the solid solution zone not only dissipates its deformation energy, but also avoids stress concentration and thus inhibits crack initiation.

In short, combining the above analysis with TEM observations, we may conclude that the solid solution formation is highly beneficial for improving the toughness of SLs.

5. Conclusion

This work verified the strengthening behavior of the single-crystalline SL coating under different deformation mechanisms. And it confirmed that the accumulation of dislocations related to phase transformation could provide more dominant strengthening than Koehler strengthening. Simultaneously, the intermixing of the interfaces greatly weakens the Koehler strengthening behavior and limits the extension of the Taylor strengthening area (the area with dislocation accumulation). Thus, we propose that the hardening of the single-crystalline SL depends on the combined effects of different strengthening mechanisms and the properties of the solid solution of the layer materials. However, the hardening behavior of single-crystalline SL, i.e., dislocation accumulation or dislocation crossing interface, are not observed in the polycrystalline SL. Consequently, polycrystalline SL generally exhibits a relatively lower hardness. Meanwhile, the solid solution formed by interfacial intermixing in the single-crystalline SL also shows phase transformations to take place, which renders the excellent toughening effect.

Declaration of Competing Interest

The authors declare that they have no known competing financial interests or personal relationships that could have appeared to influence the work reported in this paper.

Acknowledgments

This work is financially supported by FWF P 33696 (Z.C, Y.H., Z. Z). The authors thank M. Fallmann, for the thin film synthesis and SEM characterization, and the USTEM at TU Wien for the TEM sample preparation.Z.G. thanks the China Scholarship Council (CSC, 201908440933) for the support. This work is also supported by FWF I 4720 (M.B.).

Supplementary materials

Supplementary material associated with this article can be found, in the online version, at doi:10.1016/j.actamat.2022.118009.

References

[1] W. Schintlmeister, W. Wallgram, J. Kanz, Properties, applications and manufacture of wear-resistant hard material coatings for tools, Thin Solid Films 107 (2) (1983) 117–127.
[2] U. Helmersson, S. Todorova, S.A. Barnett, J.E. Sundgren, L.C. Markert, J.E. Greene, Growth of single-crystal TiN/VN strained-layer superlattices with extremely high mechanical hardness, J. Appl. Phys. 62 (2) (1987) 481–484.
[3] H. Holleck, H. Schulz, Preparation and behaviour of wear-resistant TiC/TiB_2, TiN/TiB_2 and TiC/TiN coatings with high amounts of phase boundaries, Surf. Coat. Technol. 36 (3) (1988) 707–714.
[4] H. Holleck, M. Lahres, P. Woll, Multilayer coatings—influence of fabrication parameters on constitution and properties, Surf. Coat. Technol. 41 (2) (1990) 179–190.

[5] P.B. Mirkarimi, L. Hultman, S.A. Barnett, Enhanced hardness in lattice-matched single-crystal TiN/$V_{0.6}Nb_{0.4}$N superlattices, Appl. Phys. Lett. 57 (25) (1990) 2654–2656.
[6] J.E. Sundgren, J. Birch, G. Håkansson, L. Hultman, U. Helmersson, Growth, structural characterization and properties of hard and wear-protective layered materials, Thin Solid Films 193-194 (1990) 818–831.
[7] L. Hultman, M. Shinn, P.B. Mirkarimi, S.A. Barnett, Characterization of misfit dislocations in epitaxial (001)-oriented TiN, NbN, VN, and (Ti,Nb) N film heterostructures by transmission electron microscopy, J. Cryst. Growth 135 (1) (1994) 309–317.
[8] P.C. Yashar, W.D. Sproul, Nanometer scale multilayered hard coatings, Vacuum 55 (3) (1999) 179–190.
[9] M. Kobayashi, Y. Doi, TiN and TiC coating on cemented carbides by ion plating, Thin Solid Films 54 (1) (1978) 67–74.
[10] W.D. Nix, Mechanical properties of thin films, Metall. Trans. A 20 (11) (1989) 2217.
[11] J.E. Sundgren, Structure and properties of TiN coatings, Thin Solid Films 128 (1) (1985) 21–44.
[12] R.G. Hoagland, R.J. Kurtz, C.H. Henager, Slip resistance of interfaces and the strength of metallic multilayer composites, Scr. Mater. 50 (6) (2004) 775–779.
[13] G.S. Was, T. Foecke, Deformation and fracture in microlaminates, Thin Solid Films 286 (1) (1996) 1–31.
[14] P.M. Anderson, C. Li, Hall-Petch relations for multilayered materials, Nanostruct. Mater. 5 (3) (1995) 349–362.
[15] J.D. Embury, J.P. Hirth, On dislocation storage and the mechanical response of fine scale microstructures, Acta Metall. Mater. 42 (6) (1994) 2051–2056.
[16] M.A. Phillips, B.M. Clemens, W.D. Nix, A model for dislocation behavior during deformation of Al/Al_3Sc (fcc/L12) metallic multilayers, Acta Mater. 51 (11) (2003) 3157–3170.
[17] A. Misra, J.P. Hirth, R.G. Hoagland, Length-scale-dependent deformation mechanisms in incoherent metallic multilayered composites, Acta Mater. 53 (18) (2005) 4817–4824.
[18] J.S. Koehler, Attempt to design a strong solid, Phys. Rev. B 2 (2) (1970) 547–551.
[19] S.I. Rao, P.M. Hazzledine, Atomistic simulations of dislocation–interface interactions in the Cu-Ni multilayer system, Philos. Mag. A 80 (9) (2000) 2011–2040.
[20] X. Chu, S.A. Barnett, Model of superlattice yield stress and hardness enhancements, J. Appl. Phys. 77 (9) (1995) 4403–4411.
[21] Z. Chen, Y. Zheng, Y. Huang, Z. Gao, H. Sheng, M. Bartosik, P.H. Mayrhofer, Z. Zhang, Atomic-scale understanding of the structural evolution of TiN/AlN superlattice during nanoindentation— Part 1: deformation, Acta Materialia (2022) 118008.
[22] H. Xiang, H. Li, T. Fu, Y. Zhao, C. Huang, G. Zhang, X. Peng, Molecular dynamics simulation of AlN thin films under nanoindentation, Ceram. Int. 43 (5) (2017) 4068–4075.
[23] R.F. Zhang, S. Veprek, Deformation paths and atomistic mechanism of B4→B1 phase transformation in aluminium nitride, Acta Mater. 57 (7) (2009) 2259–2265.
[24] V.I. Ivashchenko, P.E.A. Turchi, R.V. Shevchenko, L. Gorb, J. Leszczynski, First-principles investigations of the pressure-induced phase transformations and properties of crystalline and amorphous AlN, Phys. Rev. Mater. 4 (11) (2020) 113605.
[25] R.F. Zhang, S.H. Sheng, S. Veprek, Mechanism of the B3 to B1 transformation in cubic AlN under uniaxial stress, Phys. Rev. B 76 (7) (2007) 075208.
[26] D.G. Sangiovanni, F. Tasnádi, L.J.S. Johnson, M. Odén, I.A. Abrikosov, Strength, transformation toughening, and fracture dynamics of rocksalt-structure $Ti_{1-x}Al_xN(0\leq x\leq 0.75)$ alloys, Phys. Rev. Mater, 4 (3) (2020) 033605.
[27] N. Koutná, L. Löfler, D. Holec, Z. Chen, Z. Zhang, L. Hultman, P.H. Mayrhofer, D.G. Sangiovanni, Atomistic mechanisms underlying plasticity and crack growth in ceramics: a case study of AlN/TiN superlattices, Acta Mater. 229 (2022) 117809.
[28] X. Gu, Z. Zhang, M. Bartosik, P.H. Mayrhofer, H. Duan, Dislocation densities and alternating strain fields in CrN/AlN nanolayers, Thin Solid Films 638 (2017) 189–200 (Supplement C).
[29] R.F. Zhang, S.H. Sheng, S. Veprek, Mechanism of the $B3$ to $B1$ transformation in cubic AlN under uniaxial stress, Phys. Rev. B 76 (7) (2007) 075208.
[30] D. Chen, X.L. Ma, Y.M. Wang, Thickness-dependent structural transformation in the AlN film, Acta Mater. 53 (19) (2005) 5223–5227.
[31] A. Madan, I.W. Kim, S.C. Cheng, P. Yashar, V.P. Dravid, S.A. Barnett, Stabilization of Cubic AlN in Epitaxial AlN/TiN Superlattices, Phys. Rev. Lett. 78 (9) (1997) 1743–1746 .
[32] Z. Zhang, Z. Chen, D. Holec, C.H. Liebscher, N. Koutná, M. Bartosik, Y. Zheng, G. Dehm, P.H. Mayrhofer, Mapping the mechanical properties in nitride coatings at the nanometer scale, Acta Mater. 194 (2020) 343–353.
[33] Z. Chen, D. Holec, M. Bartosik, P.H. Mayrhofer, Z. Zhang, Crystallographic orientation dependent maximum layer thickness of cubic AlN in CrN/AlN multilayers, Acta Mater. 168 (2019) 190–202.
[34] K. Yalamanchili, F. Wang, H. Aboulfadl, J. Barrirero, L. Rogström, E. Jiménez-Pique, F. Mücklich, F. Tasnadi, M. Odén, N. Ghafoor, Growth and thermal stability of TiN/ZrAlN: effect of internal interfaces, Acta Mater. 121 (2016) 396–406 Supplement C.
[35] S.H. Jhi, S.G. Louie, M.L. Cohen, J.W. Morris, Mechanical instability and ideal shear strength of transition metal carbides and nitrides, Phys. Rev. Lett. 87 (7) (2001) 075503.
[36] U. Wahlström, L. Hultman, J.E. Sundgren, F. Adibi, I. Petrov, J.E. Greene, Crystal growth and microstructure of polycrystalline $Ti_{1-x}Al_xN$ alloy films deposited by ultra-high-vacuum dual-target magnetron sputtering, Thin Solid Films 235 (1) (1993) 62–70.
[37] M. Zhou, Y. Makino, M. Nose, K. Nogi, Phase transition and properties of Ti–Al–N thin films prepared by r.f.-plasma assisted magnetron sputtering, Thin Solid Films 339 (1) (1999) 203–208.
[38] B. Grossmann, N. Schalk, C. Czettl, M. Pohler, C. Mitterer, Phase composition and thermal stability of arc evaporated $Ti_{1-x}Al_xN$ hard coatings with $0.4\leq x\leq 0.67$, Surf. Coat. Technol. 309 (2017) 687–693.
[39] K. Kutschej, P.H. Mayrhofer, M. Kathrein, P. Polcik, R. Tessadri, C. Mitterer, Structure, mechanical and tribological properties of sputtered $Ti_{1-x}Al_xN$ coatings with $0.5\leq x\leq 0.75$, Surf. Coat. Technol. 200 (7) (2005) 2358–2365.
[40] A. Hörling, L. Hultman, M. Odén, J. Sjölén, L. Karlsson, Mechanical properties and machining performance of $Ti_{1-x}Al_xN$-coated cutting tools, Surf. Coat. Technol. 191 (2) (2005) 384–392.
[41] P.H. Mayrhofer, D. Music, J.M. Schneider, Influence of the Al distribution on the structure, elastic properties, and phase stability of supersaturated $Ti_{1-x}Al_xN$, J. Appl. Phys. 100 (9) (2006) 094906.
[42] M. Stueber, H. Holleck, H. Leiste, K. Seemann, S. Ulrich, C. Ziebert, Concepts for the design of advanced nanoscale PVD multilayer protective thin films, J. Alloy. Compd. 483 (1) (2009) 321–333.
[43] M. Fallmann, Z. Chen, Z.L. Zhang, P.H. Mayrhofer, M. Bartosik, Mechanical properties and epitaxial growth of TiN/AlN superlattices, Surf. Coat. Technol. 375 (2019) 1–7.
[44] G.I. Taylor, The mechanism of plastic deformation of crystals. Part I.—Theoretical, Proc. R. Soc. Lond. Ser. A 145 (855) (1934) 362–387 Containing Papers of a Mathematical and Physical Character.
[45] B. Devincre, L. Kubin, T. Hoc, Physical analyses of crystal plasticity by DD simulations, Scr. Mater. 54 (5) (2006) 741–746.
[46] M.B. Kanoun, S. Goumri-Said, Effect of alloying on elastic properties of ZrN based transition metal nitride alloys, Surf. Coat. Technol. 255 (2014) 140–145.
[47] E.S. Pacheco, T. Mura, Interaction between a screw dislocation and a bimetallic interface, J. Mech. Phys. Solids 17 (3) (1969) 163–170.
[48] C.-S. Shin, D. Gall, N. Hellgren, J. Patscheider, I. Petrov, J.E. Greene, Vacancy hardening in single-crystal TiN_x(001) layers, J. Appl. Phys. 93 (10) (2003) 6025–6028.
[49] T. Lee, K. Ohmori, C.S. Shin, D.G. Cahill, I. Petrov, J.E. Greene, Elastic constants of single-crystal TiN_x(001) ($0.67\leq x\leq 1.0$) determined as a function of x by picosecond ultrasonic measurements, Phys. Rev. B 71 (14) (2005) 144106.
[50] A. Leyland, A. Matthews, On the significance of the H/E ratio in wear control: a nanocomposite coating approach to optimised tribological behaviour, Wear 246 (1) (2000) 1–11.
[51] Q. Xia, H. Xia, A.L. Ruoff, Pressure-induced rocksalt phase of aluminum nitride: a metastable structure at ambient condition, J. Appl. Phys. 73 (12) (1993) 8198–8200.
[52] M. Mikula, D. Plašienka, D.G. Sangiovanni, M. Sahul, T. Roch, M. Truchlý, M. Gregor, L.u. Čaplovič, A. Plecenik, P. Kúš, Toughness enhancement in highly NbN-alloyed Ti-Al-N hard coatings, Acta Mater. 121 (2016) 59–67.
[53] L. Zhou, D. Holec, P.H. Mayrhofer, Ab initio study of the alloying effect of transition metals on structure, stability and ductility of CrN, J. Phys. D Appl. Phys. 46 (36) (2013) 365301.
[54] D. Holec, L. Zhou, R. Rachbauer, P.H. Mayrhofer, Alloying-related trends from first principles: An application to the Ti–Al–X–N system, J. Appl. Phys. 113 (11) (2013) 113510.
[55] D.G. Sangiovanni, L. Hultman, V. Chirita, Supertoughening in B1 transition metal nitride alloys by increased valence electron concentration, Acta Mater. 59 (5) (2011) 2121–2134.